IEEE Access
Multidisciplinary | Rapid Review | Open Access Journal

Received 5 June 2023, accepted 29 June 2023, date of publication 4 July 2023, date of current version 11 July 2023.

Digital Object Identifier 10.1109/ACCESS.2023.3292304

RESEARCH ARTICLE

Ultra-High Input Impedance Buffer for Dry or Capacitive Electrodes: Design and Characterization for Industry

ROBERT CAMÓS-VIDAL AND JAVIER ROSELL-FERRER, (Senior Member, IEEE)
Department of Electronic Engineering, Polytechnic University of Catalunya, Catalunya, 08034 Barcelona, Spain
Corresponding author: Robert Camós-Vidal (Robert.camos@upc.edu)

ABSTRACT A large number of health and wellness applications wish to monitor electrocardiogram signal (ECG) in the least intrusive way possible. The use of dry textile electrodes with high input impedance bio-amplifiers is a common technique. This paper presents a novel ultra-high input impedance buffer to obtain a reduced input capacitance and enhance the acquisition of results for dry or non-contact capacitive ECG electrodes. Based on different bootstrapping techniques, input stage biasing and unipolar power supply, an operational amplifier buffer is implemented on Printed Circuit Board (PCB) to provide a low cost solution. The solution considers the protections for electrostatic discharges (ESD) and filters for interferences, maintaining high input impedance design. A method to measure input impedances in the range of femtofarads is also proposed. This active electrode prototype presents a 191 fF input capacitance at 50 Hz. Different skin-electrode impedance cases are studied to obtain the Common Mode Rejection Ratio (CMRR). As a result, a value of 81.4 dB is obtained with zero mismatch and 76.1 dB at 50 Hz is obtained with a resistive mismatch of 1-2.2 MΩ. Moreover, ECG test is evaluated using a discrete back-end circuit, digital filtering and software display. Finally, the full ECG circuit has been simulated under an ESD transient of ±8 kV IEC 61000-4-2 waveform. This paper demonstrated that the proposed solution with standard discrete components fulfills the industry requirements for robust ultra-high impedance ECG sensor.

INDEX TERMS Biomedical monitoring, capacitive electrodes, dry electrodes, electrocardiogram (ECG), ESD protections, non-contact, ultra-high input impedance.

I. INTRODUCTION

A huge number of applications are demanding a new generation of non-invasive sensors to be applied in several fields such as medicine, fitness, industry 4.0 or daily smart devices. The miniaturization of electronic integrated circuits, new flexible printed circuit technologies, advanced electronic textiles and ultra-low consumption wireless communications have promoted the emergence of a wide portfolio of new applications.

These portable smart devices try to adapt to the changes of the population's life habits, like the growing market for the monitoring of body vital signs. The heart rate, SpO2, sleep and stress have been commonly used in several situations of people's common life, first aid, clinical consultation, sport club or personal life.

During the last decade, the new cardiac solutions commonly use dry or textile electrodes with patient comfort, low cost and high integration capabilities.

Nevertheless, this type of electrodes degrades the quality of the register, compared to standard Ag/AgCl electrodes, due to its high electrical impedance, and cannot be suitable for long-term monitoring owing to serious skin irritations or allergies appearing after its use [1].

The need for non-invasive ECG sensors for long-term monitoring has resulted in a lengthy effort in scientific research to developed different types of non-contact electrodes based on capacitive coupling. Recently, several studies have emerged which focus on mobility, home-resting and wearable solutions. The following studies show practical examples of

The associate editor coordinating the review of this manuscript and approving it for publication was Venkata Rajesh Pamula.

implementation of non-contact electrodes on car seats [2], sofa resting [3] and wearables [4], [5].

Many well-known techniques and technologies in the field of active electrodes have been combined and improved in recent studies. For example, the PS25251 EPIC commercialized a capacitive electrode [6], which uses the positive feedback technique to reduce the input sensor capacitance, and it was tested as a wearable solution [7].

Another interesting solution is presented in [8], where an ultra-high input impedance is achieved by applying a two wired electrode with bootstrapping power supply [9], [10]. Badarov et al. [11] proposed an advanced bootstrapping buffer feedback to increase the impedance that also integrates a basic electrostatic discharge (ESD) protection

The paper [12] proposes a remarkable fitted solution and fabricated an ultrathin electrode with Thinned flexible Si-OpAmps.

Finally, two examples of full custom design of active electrodes in silicon integrated circuits (IC) are shown. The first one [13], explains the development of the bootstrapped unit gain buffer with positive feedback to reduce Cin without the use of neutralization or manual tuning. The second IC paper [14] presents a similar circuitry of positive feedback and, in addition, a DC-servo loop for the input polarization allowing for a faster recovery after a transient at the input. In this case, each active electrode uses an instrumentation amplifier with a gain of 10 and the manual adjustment of the feedback loop is required.

The current paper presents the design of an active electrode with power supply bootstrapping; as a solution for ultra-high impedance electrodes for electrocardiography using dry electrodes or capacitive electrodes. In contrast with previous academic proposals, we introduced the ESD protection which fulfills the required global industry standard. This regulatory test reaches a higher voltage peak than any internal protection of the IC solutions on the market can support.

Furthermore, no manual adjusting is required and loop stability is ensured for wide unbalanced input impedances with the patient.

The Common Mode Rejection Ratio (CMRR) is evaluated for realistic impedance mismatch and a new method to measure the input impedance in the range of femtofarads is proposed.

II. SENSOR DESIGN

The current section describes the key characteristics of the proposed electronic circuit and their electronic implementation. The required specifications are:

- Differential amplification.
- Auto Bias of inputs to allow capacitive electrodes.
- High CMRR also for high electrode impedance mismatch.
- Protections against ESD.
- Minimum number of connections between the active electrode and the amplification stage.

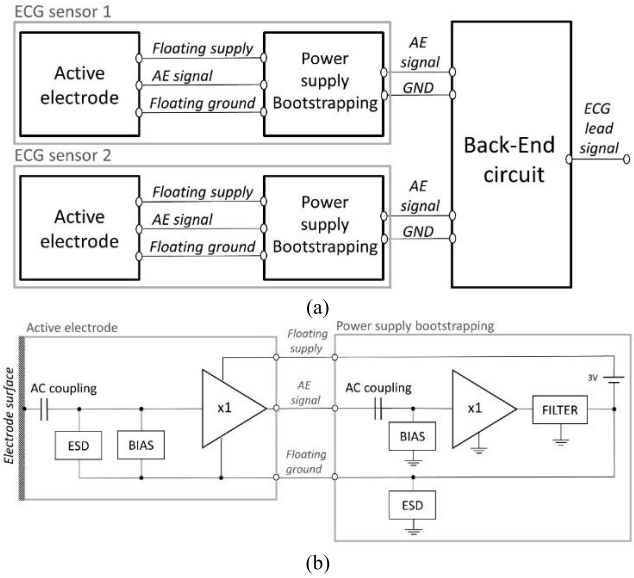

FIGURE 1. Block diagram of the proposed ECG solutions: (a) three main blocks (b) detailed functional block of the ECG sensor.

The proposed design is a flexible and modulable solution based on three to five different PCBs and the minimal necessary cables, Figure 1(a). This allows it to be adjusted for many different types of real applications.

A complete solution for a differential ECG lead is composed of two ECG sensors connected to a back-end circuit, see Figure 1(a).

Both ECG sensors are composed of two parts: active electrode and power supply bootstrapping, Figure 1(b). The active electrode PCB is wired to the power supply bootstrapping through three wires: floating supply, floating GND and signal. Other studies use only two wires for the active electrode [8] but they are not valid for capacitive electrodes.

Then, each sensor uses two-wires (signal and GND) connecting the power supply bootstrapping to the back-end circuitry.

A. ACTIVE ELECTRODE (AE)

The schematic circuit of the proposed active electrode is shown in Figure 2.

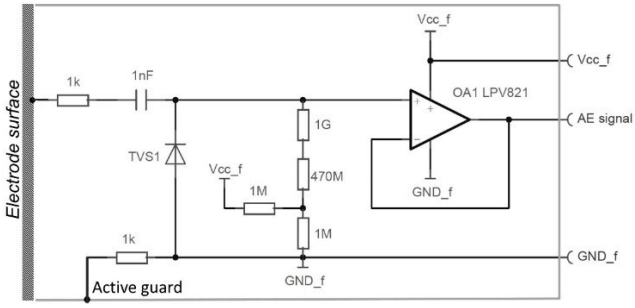

FIGURE 2. Proposed active electrode.

The signal acquisition is done through the electrode plate, which is made with a circular copper surface of a two-layers

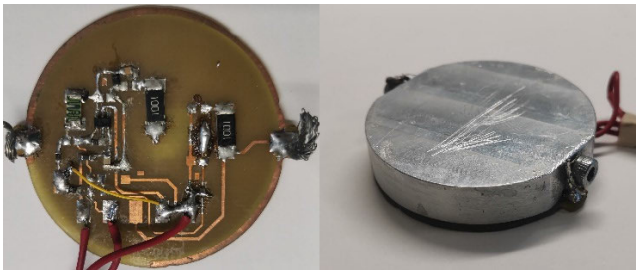

FIGURE 3. Implemented ECG sensor: Layout on left and active shielding on right (diameter of 42.4 mm and height of 10 mm).

printed circuit board, see Figure 3. The circuit layout was designed with additional footprints to allow changes in the components during the electrode validation.

A 42.4-mm in diameter plate fully covers the bottom layer of the PCB. The circuit of the active electrode remains on the top layer. A 1 nF series capacitor is directly connected to the plate providing an AC-coupling when non-capacitive electrodes are used to avoid the effect of DC potentials at the electrodes.

The electrode is basically a voltage follower based on an operational amplifier, the AD8505 of Analog Devices was selected (OA1) for its specifications [15], besides a very low current consumption (20 μA) and 1.8-5 V of single supply, this OA provides other important characteristics required for bio-signal acquisition: rail to rail input/output, 105 dB CMRR, 1 pA input bias current, low voltage/current noise and high input impedances (220 GΩ || 4.2 pF).

The input biasing circuit of the AD8505 is connected to half of the OA supply voltage with two resistors with a total value of 1.47 GΩ.

Finally, an aluminum case covers the top circuit layer, containing all the electronics, to protect them from external interferences. This case is used as an active guard and it is connected to the floating bootstrapped GND.

B. POWER SUPPLY BOOTSTRAPPING

The power supply bootstrapping is presented in Figure 4 and the three external connections are wired directly to the active electrode (Figure 2).

The power supply of the active electrode (OA1) is brought by a bootstrapping circuit. Providing a fixed supply voltage with a floating GND, which follows the AC voltage of the input signal. Due to this power bootstrapping, in theory, the AC input impedance of the active electrode will be infinite [9], [10].

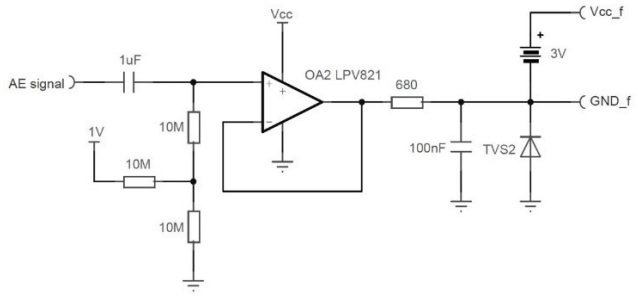

FIGURE 4. Power supply bootstrapping circuit for each active electrode.

The active electrode signal passes through a first order high pass filter (corner frequency of 0.01 Hz) and is forced to be DC shifted, 500 mV above ground. This voltage divider is used as a DC shift of signal and at the same time enables input biasing of the second buffer OA2.

OA2 buffer output is the floating reference for the active electrode (GND_f). This signal is filtered with an RC low pass filter to assure the feedback loop stability at high-frequencies.

A 3V battery connected to GND_f provides a unipolar power supply, whereas both supply nodes (Vcc_f and GND_f) follow the signal voltage variations.

C. ESD PROTECTION CIRCUIT

Silicon-basic ESD protection, for the input specific pins, are usually integrated in the last generation of Analog Front-End (AFE) and bio-amplifiers designed for medical devices applications. This basic circuitry protects against transients of limited amounts of energy, normally based on the Human Body Model (HBM) or Charge Device Model (1 kV up to 4kV peaks) [16].

Nevertheless, the global EMC directives require to pass assays with significantly higher amounts of energy, such as the international standard IEC 61000-4-2 [17].

The OA1 (AD8505) has clamping diodes integrated as transient voltage protection. The manufacturer specifies that these diodes, in direct conduction, support a limit current up to 10 mA, whenever the voltage exceeds 0.5 V over the power supply rail [15].

These reduced dimensionally CMOS protections are limited protection and have to be complemented with extern powerfully transient suppressor [18], [19], [20], as a way to support the high ESD of IEC standards and avoid damage to the operational amplifier.

In this case, we selected a unidirectional TVS diode to conform to the ESD main protection. The ESD7351 is carefully chosen in order to preserve the ultra-high input impedance of the sensor (±20 kV IEC 61000-4-2, $V_{RWM} = 3.3$ V, $I_R = 1$ nA and a junction capacitance of 0.6 pF) [21]. Very low values of leakage current and capacitance are essential features to achieve a proper ESD protection for this application.

Our proposal is to use two TVS (see Figure 1 and Figure 2) to ensure a safe path for ESD transients avoiding the degradation of the input impedance. The TVS1 gives an ESD transient path from the input to the floating ground and TVS2 drives the transients from the floating bootstrapped GND_f to the general GND of the circuit.

D. BACK-END CIRCUIT

The differential ECG amplifier was implemented with a commercial instrumentation amplifier, Figure 5.

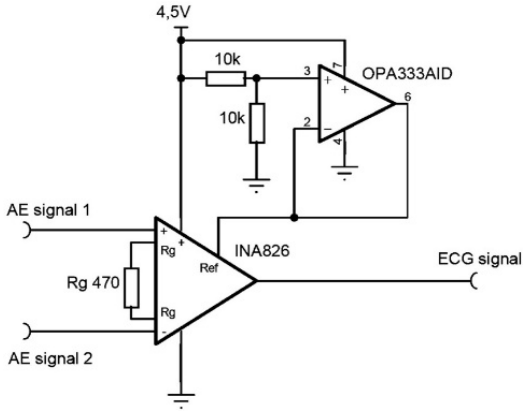

FIGURE 5. Instrumentation amplifier with middle voltage reference based on the INA826.

Based on the evaluation board INA826EVM of Texas Instruments, the INA826 instrumentation amplifier (IA) has adjusted to obtain a differential ECG signal from two designed bootstrapped active electrodes (Figure 1 (a)) with an IA gain of 106 and an offset of 2.25 V at the output.

These gain and offset adjustments are chosen to easily measure the ECG output signal with an oscilloscope or to digitalize it with unipolar analog-to-digital converters.

III. SIMULATIONS OF ESD

The evaluation of the protection circuit against ESD has been done through PSPICE simulations. Using TINA-TI software, we simulated a complete circuit of an ECG sensor (active electrode with power supply bootstrapping) together with an ESD generator.

The generation of the ESD discharge has been emulated with passive components. The first simulation shows how this generator is set to the ±8 kV IEC 61000-4-2 waveform specs [17], [22]. Following the simplified model of the current measurement setup defined in this standard [23], a 2 Ω load resistor is used for ESD transient discharge; see Figure 6.

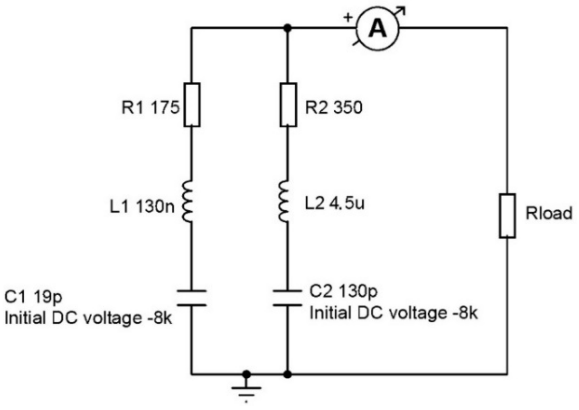

FIGURE 6. Simplified circuit of current measurement setup for IEC 61000-4-2.

The obtained current waveform of this ESD circuit generator is shown in Figure 7.

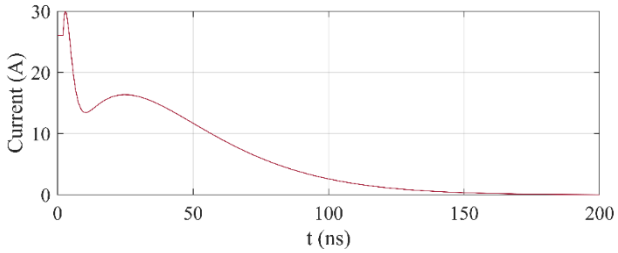

FIGURE 7. Simulation results: ESD current waveform of ESD generator emulation circuit.

Once we fitted the discharge curve, the proposed ECG sensor circuit was tested with this ESD generator in order to analyze the protection of this circuit against voltage transients.

The simulation of a complete system has been done connecting the ESD simulator of Figure 6 directly to the active electrode path in Figure 1(b).

Connected to the circuit, the transient response of the ESD model maintains the shape discharge and the peaks are of 6.39 kV and 6.35 A.

As expected, the energy absorption of ESD are mainly done through the protections and so the AD8505 input buffer received the residual amount of the ESD transient energy with a limited voltage and current ($V < 3.83$ V and $I < 7$ mA), see Figure 8.

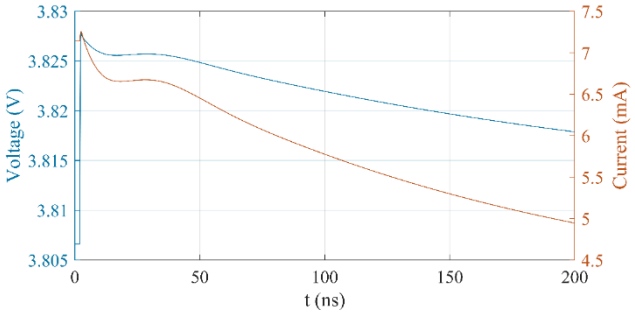

FIGURE 8. Input buffer signals: voltage and current.

The input buffer voltage does not exceed the maximum supply nor the input specifications of the manufacturer [15]. Moreover, the current through integrated clamping diodes remain under the limit of 10 mA.

Thus, the protection circuit against ESD fulfills the main purpose and preserves the ultra-high input impedance for the final application.

IV. MEASUREMENTS AND RESULTS

The measurement of input impedances in the range of fF at low frequencies is not simple. For this reason, we will describe in detail the measurement methods and the test setups.

Based on the previous studies, a new method is proposed to reduce the capacitive parasite effects of surrounding structures and also improve the susceptibility from external interference.

As a result of the proposed setup, the characterization of ultra-high input impedances and the CMRR evaluation could be performed with precision when applying high output impedance sources.

A. INPUT IMPEDANCE MEASUREMENT

1) PROPOSED SETUP

Most studies on ultra-high input impedance active electrodes have only been limited to verifying the quality of ECG signal of the implemented circuit. Only few of them actually configure a test to measure the real input impedance of the sensor.

These are commonly performed by adding an additional high impedance in series to the buffer [8], [13], [24], usually a giga-ohm resistor (R_s). Moreover, an input guard is also used as a shielding against EMIs and external capacitive parasite coupling, for example the main power interferences. This setup is shown in Figure 9.

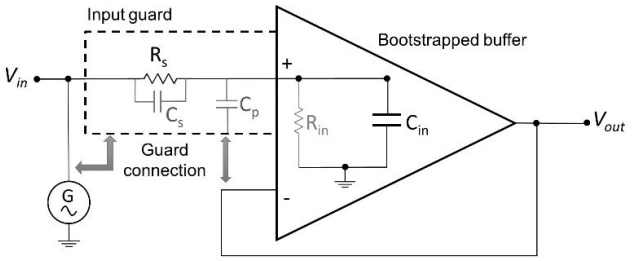

FIGURE 9. Standard setup to measure ultra-high input impedance.

Using this setup topology, the input impedance of a bootstrapped OA (Z_{in}) could be calculated as a simple voltage divisor of impedances (1).

$$Z_{in} = \frac{R_s \cdot \frac{V_{out}}{V_{in}}}{1 - \frac{V_{out}}{V_{in}}} \tag{1}$$

Nevertheless, this method could give an inaccurate value of the input impedance. The cause is two undesired capacitances, showed in Figure 9, C_p and C_s:

The coupled capacitance between the input guard and the electrode surfaces (Cp):

It will be necessary to consider the effect of C_p, if the design of this guard has a reduced size or close distance to the electrode surface. As shown in Figure 9, the coupled effect of C_p will be different depending on the reference potential where the active guard is connected (input signal or output buffer signal).

When the active guard is connected to the output buffer voltage, C_p could act as a positive feedback to the OA; especially when R_s in the order of giga-ohm is used.

In the case that the guard is wired to the waveform generator G, the parasite coupling C_p will appear in parallel to the serial high-value resistor R_s. For example, this setup was used in [8]. In this case C_p appears in parallel to the parasitic capacitance (C_s).

The parallel stray capacitance of the resistor R_s (C_s) :

Any stray capacitance of 1-10 pF in front of a series giga-ohm resistor is quite similar in impedance magnitude at the ECG spectrum frequencies: i.e. 1 pF at 100 Hz has a magnitude of 1.6 GΩ. As this parasite capacitance C_s is in parallel to R_s, the total series impedance must be considered when using the equation (1).

Moreover, the impedance magnitude of C_s could be similar to the input capacitance (C_{in}) and so a capacitive voltage divider also appears on the measurement and the equation (1) is not applicable.

Thus, the measurement based on the equation (1) and Figure 9 is nonrealistic. The positive feedback through setup input guard or the magnitude of series capacitive couplings on the R_s overrides the simplicity of the impedance measurement with this standard setup.

This article proposes an alternative setup for the measurement of the input impedance for capacitive electrodes. It is based on a direct AC-coupling of the input signal from the faraday chamber to the electrode surface, see Figure 10. A similar solution is adopted in the study [9], which uses a conductive sheet as signal AC-coupling.

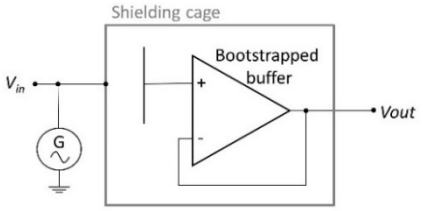

FIGURE 10. Proposed setup for the measurements of ultra-high input impedance in active electrodes.

A completely closed stainless-steel cylindrical cage of Ø60 cm x 50 cm is used to shield the active electrode. The sine wave generator is connected to its conductive cage body.

Only 3 wires come out of the cage: the output signal and the bootstrapping supply (V_{out}, V_{cc_f} and GND_f). The proposed active electrode is inside the cage and the power supply bootstrapping is outside, Figure 2 and Figure 4; respectively.

This specific setup avoids any kind of positive feedback loop, eliminates the series capacitive coupling and adds a shielding to EMI parasite couplings. Characterization of cage-electrode capacitance (C_g)

To calculate the input impedance with the proposed setup, the characterization of the AC-coupling formed between the two conductive surfaces is necessary: the cylindrical cage and the electrode surface.

Figure 11. shows the method to obtain the value for C_g based on a simple high pass filter (HPF) configuration, where R_s is known.

A plate of an electrode has been isolated from the rest of the circuitry and placed in the internal central point of the cage body. A wire soldered to the plate has been taken out of the cage and connected to a 100 kΩ resistor (Rs) pathed to

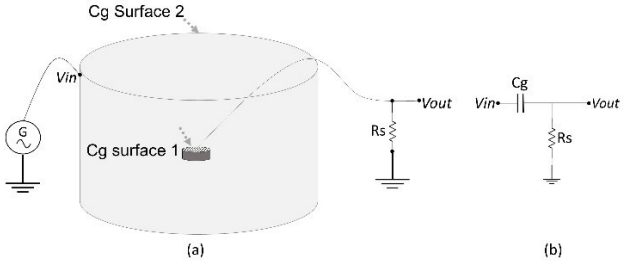

FIGURE 11. Characterization of Cg based on proposed setup: (a) Test setup. (b) Equivalent circuit.

ground. Finally, the waveform generator and an oscilloscope has been used to determine the -3 dB cutoff frequency.

The C_g value estimated with this method was 3.68 pF.

2) ELECTRODE INPUT IMPEDANCE TEST

Once the C_g is obtained, the input impedance test is performed on the two ECG sensors implemented and the input impedance calculated.

Using a PicoScope 2205 instrument, and due to the limitations of this equipment, the transfer function used to estimate the input impedance response has been obtained in several points in the frequency band from 1 to 250 Hz.

Specifically, the magnitude $|H(j\omega)| = |V_{out}/V_{in}|$ is measured from the spectrum analyzer view and the phase $\varphi = \arg(V_{out}/V_{in})$ is calculated with the signals zero-crosses in time domain view.

Following the setup of Figure 11 and the design of the active electrode Figure 2, the equations to describe the transfer function are (2).

$$\left.\begin{array}{l} H = \frac{V_{out}}{V_{in}}(j\omega) = \frac{Z_{in}}{Z_{in}+Z_s} \\ Z_s = 1000 - j\frac{1}{\omega C_g} \end{array}\right\} \rightarrow$$

$$|Z_{in}| = \sqrt{R_s^2 + {}^1\!/\!_{(\omega^2 C_s^2)}} \cdot \frac{|H|}{\sqrt{|H|^2 - 2 \cdot cos\,|H| + 1}}$$

$$\arg(Z_{in}) = \arctan\left(-\frac{1}{R_s C_s \omega}\right) + \arctan\left(\frac{\sin(\varphi)}{\cos(\varphi) - |H|}\right) \quad (2)$$

Using these equations and the previous measurements of the transfer function, we could represent the values of Z_{in} in the ECG frequency bandwidth for each active electrode, Figure 12.

The input impedance of the bootstrapped circuit shows an inductive behavior in the lowest part of the frequency range. Then, it has a capacitive behavior in parallel with a resistance. The resistance decreases with the frequency and the capacitor increases with frequency due to the reduction of feedback to ensure stability.

The small mismatch between the two ECG sensors could be caused by various reasons: passive component tolerances, variances of voltage between the bootstrapped power supplies and also the limited accuracy of phase measurements based on signal zero-crossings.

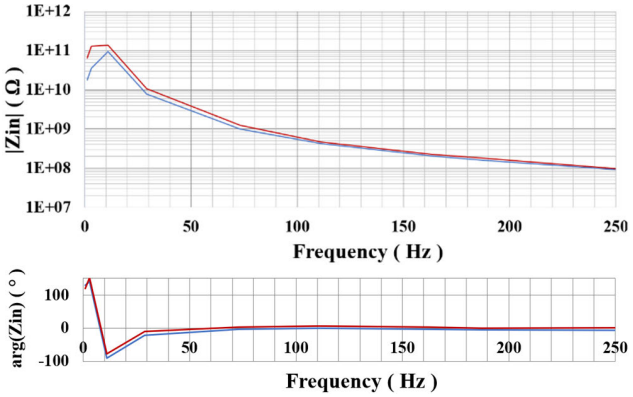

FIGURE 12. Input impedance of the two proposed active ECG electrodes.

TABLE 1. Input capacitance of proposed ECG electrode.

Frequency (Hz)	C_{in} (fF)
50	191
from 11 to 250	[9 to 820]

Finally, the Z_{in} impedance result is represented as an RC parallel model $R_{in}||\,C_{in}$ in order to calculate C_{in} and confirm the reduction of the input capacitance of the OA used as a buffer. The AD8505 operational amplifier has specified a 4.2 pF input impedance in common mode. The estimated values after the measurements and calculations are shown in TABLE 1.

The value of input capacitance has the same order of magnitude as other studies, e.g. [8], that do not use ESD protections. The proposed solution shows that it is feasible to design an ultra-high impedance electrode with integrated ESD protections, while reaching the EMC standards requirements.

B. COMMON MODE REJECTION RATIO

Following the same methodology as the setup test, the measurements of CMRR is done with the complete differential circuit for the ECG acquisition.

Two active electrodes have been placed into the center of the cage, maintaining a prudential distance between them. Different series impedances, resistors or capacitors, have been soldered into the plate of each electrode in order to force input balance and unbalance impedances between the

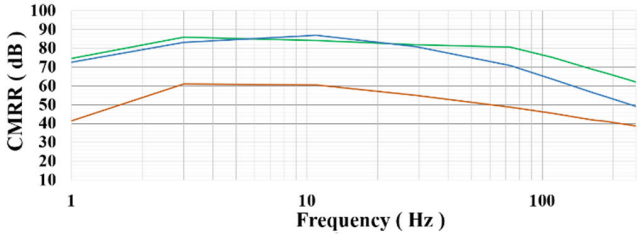

FIGURE 13. CMMR test results: 1 MΩ conductive balance (green), 1-2.2 MΩ conductive unbalance (blue) and 34-56 pF capacitive unbalance tests (orange).

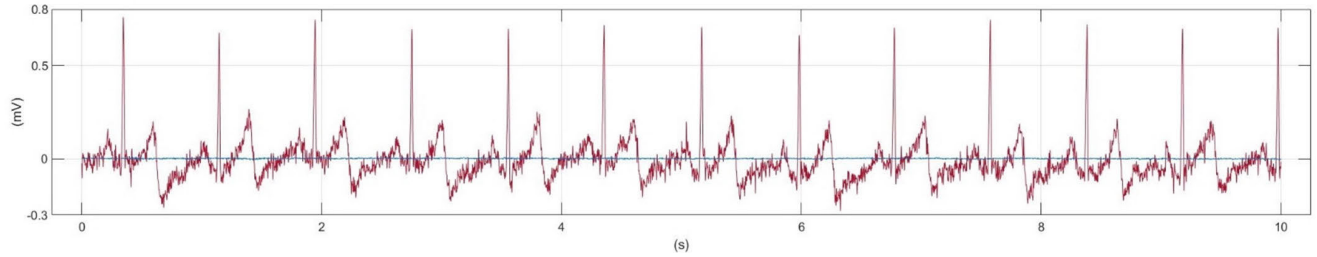

FIGURE 14. ECG signal acquisition (red) of the proposed circuit through a cotton shirt, and the noise of the system (blue) with the electrodes short-circuited.

ECG sensors. The two respective power supply bootstrapping and the back-end circuits have been connected to them, but outside of the cage.

Different tests have been performed to evaluate the behavior of the proposed solution under realistic acquisition situations, see Figure 13:

- Good conductive dry electrodes (balanced impedances): 1 MΩ series resistors in both input sensors.
- Partial conductive dry contact (unbalanced impedances): 1 MΩ in one sensor and 2.2 MΩ series resistors in the other.
- Partial capacitive contact (unbalanced impedances): 34 pF in one sensor and 56 pF in the other.

In the case of the capacitive contact, the unbalanced impedance setup considers a contact with the person through a T-shirt (350 μm cotton) on both electrodes and the unbalanced case contemplates a full body-electrode surface contact with a dry cotton dielectric in one electrode (56 pF) and a partial contact (59% of the area) in the other electrode (34 pF).

The CMRR results obtained with balanced and unbalanced impedances are shown in Figure 13. For dry electrodes, despite the input impedance mismatching, these results are really similar up to 100 Hz, where the difference is less than 10 dB. In this case, the effect of unbalanced conditions is noticed in the high frequency band with a significant decrease.

Otherwise, the unbalanced capacitive test shows how the CMRR is degraded. The unbalanced conductive CMRR value is maintained low in the frequency band up to 100 Hz, 25 dB below in comparison with the previous conductive conditions. This CMRR difference is reduced to 10 dB over 100 Hz.

TABLE 2 summarizes the CMRR result values of the three tests. These results are high considering the magnitude of input electrode impedances and the important mismatches of 100% of the values. The use of the driven right leg (DRL) method could also be used obtaining a higher effective CMRR. A clear example of this is reference [14], where 30 dB CMRR electrodes were designed and an effective CMRR of 70 dB were obtained with the DRL technique.

C. BIOPOTENTIAL & NOISE MEASUREMENTS

Last measurements are the acquisition of ECG signal and the noise level in order to validate the proposed solution as an ECG monitoring system with non-direct contact with the skin.

TABLE 2. CMMR test results.

Frequency (Hz)	Conductive balanced (dB)	Conductive unbalanced (dB)	Capacitive unbalanced (dB)
50	81.4	76.1 dB	51.9 dB
1 to100	[74.6 to 85.9]	[65.7 to 87.1]	[41.5 to 61.0]
100 to 250	[62.3 to 76.7]	[49.3 to 65.7]	[38.8 to 46.7]

Like the previous CMRR test, the measurement is done with the proposed circuit of Figure 1. In this case, each sensor has been attached to the patient's cotton shirt by the weight of every forearm. Likewise, an additional Ag/AgCl electrode has been used in accordance with Einthoven's triangle, so attached on the patient's left leg. This third electrode equalizes the patient's body potential to the GND circuit, avoiding long saturation of the system when the patient is accidentally disconnected.

The acquired ECG signal of a subject through a cotton shirt is shown Figure 14. The signal has been digitally low pass filtered at 100 Hz. As it can be seen, looking at the drift of the base line, the corner frequency of the actual high pass filter is in the order of 0.1 Hz due to the small capacitance of the electrode through a cotton shirt. The measured voltage of the output in this case is 117.1 μV (rms). To measure the intrinsic noise of the system both electrodes were connected together and the measured output was 3.71 μV (rms) giving an approximate Signal to Noise Ratio of 31 dB.

V. CONCLUSION

The current paper proposes a modulable ECG solution, based on a minimal number of wires between the stages, that could be implemented in a single PCB or distributed in up to five blocks. This typology allows it to be adjusted in different fields of applications, such as wearable, mobility or home resting. Besides, a wide range of electrode designs could be supported with this AC-coupled electrode, either textile, dry or capacitive.

A new test setup is proposed for the accurate characterization of the sensor. As a result, the femtofarads input capacitance is estimated in the ECG frequency range. Also, a high CMRR is obtained and measured in different cases: balanced/unbalanced and resistive/capacitive contact.

To further increase the CMRR, it is possible to use the Driven Right Leg technique (DRL), as in [14].

No manual adjusting is required and the stability of bootstrapped active electrodes is guaranteed by the use of a unit gain stage.

Finally, the ESD protection is designed to ensure the IEC standard. The simulation results of the ECG sensor corroborated the full protection against ESD transients.

Therefore, the design robustness of the proposed ECG ultra-high input impedance electrode is proven, thereby validating the feasibility of solution for industrial application.

REFERENCES

[1] T. W. Degen, "Portable devices for mobile health monitoring," DSc dissertation, Dept. Inf. Technol. Elect. Eng., Neuchâtel Univ., Oberwil, Switzerland, 2011.

[2] T. Torfs, A. Patel, and I. D. Castro, "Active capacitive ECG system with all-digital 'driven right leg' common mode suppression," in *Proc. IEEE Biomed. Circuits and Syst. Conf. (BioCAS)*, Oct. 2021, pp. 01–04, doi: 10.1109/BioCAS49922.2021.9644964.

[3] Y. Jang, S. Kim, K. Kim, and D. Yoo, "A study of sofa-type capacitive coupling electrocardiograph system to measure stress relief for sleeping or resting with oxygen taking," in *Proc. 42nd Annu. Int. Conf. IEEE Eng. Med. Biol. Soc. (EMBC)*, Jul. 2020, pp. 4547–4550, doi: 10.1109/EMBC44109.2020.9176113.

[4] T. Wang, H. Zhang, and S. Lin, "Influence of capacitive coupling on high-fidelity non-contact ECG measurement," *IEEE Sensors J.*, vol. 20, no. 16, pp. 9265–9273, Aug. 2020, doi: 10.1109/JSEN.2020.2986723.

[5] B. Babusiak, S. Borik, and L. Balogova, "Textile electrodes in capacitive signal sensing applications," *Measurement*, vol. 114, pp. 69–77, Jan. 2018, doi: 10.1016/j.measurement.2017.09.024.

[6] *PS25251 EPIC QFN Sensor, Electrophysiology, High Gain Datasheet*, document 291766 V5, Plessey Plymouth, U.K.

[7] M. Stork and J. Houzar, "Non-contact ECG monitoring for driver," in *Proc. 30th Int. Conf. Radioelektronika (Radioelektronika)*, 2020, pp. 1–5, doi: 10.1109/RADIOELEKTRONIKA49387.2020.9092405.

[8] F. N. Guerrero and E. M. Spinelli, "A two-wired ultra-high input impedance active electrode," *IEEE Trans. Biomed. Circuits Syst.*, vol. 12, no. 2, pp. 437–445, Apr. 2018.

[9] J. M. Kootsey and E. A. Johnson, "Buffer amplifier with femtofarad input capacity using operational amplifiers," *IEEE Trans. Biomed. Eng.*, vols. BME–20, no. 5, pp. 389–391, Sep. 1973.

[10] S. Lanyi and M. Pisani, "A high-input-impedance buffer," *IEEE Trans. Circuits Syst. I, Fundam. Theory Appl.*, vol. 49, no. 8, pp. 1209–1211, Aug. 2002.

[11] D. H. Badarov, G. S. Mihov, and I. T. Iliev, "Development of analog front-end for capacitive ECG signal acquisition," in *Proc. 30th Int. Sci. Conf. Electron. (ET)*, 2021, pp. 1–4, doi: 10.1109/ET52713.2021.9579902.

[12] Y. Gao, V. V. Soman, J. P. Lombardi, P. P. Rajbhandari, T. P. Dhakal, D. G. Wilson, M. D. Poliks, K. Ghose, J. N. Turner, and Z. Jin, "Heart monitor using flexible capacitive ECG electrodes," *IEEE Trans. Instrum. Meas.*, vol. 69, no. 7, pp. 4314–4323, Jul. 2020, doi: 10.1109/TIM.2019.2949320.

[13] Y. M. Chi, C. Maier, and G. Cauwenberghs, "Ultra-high input impedance, low noise integrated amplifier for noncontact biopotential sensing," *IEEE J. Emerg. Sel. Topics Circuits Syst.*, vol. 1, no. 4, pp. 526–535, Dec. 2011, doi: 10.1109/JETCAS.2011.2179419.

[14] M. Chen, H. S. Chun, I. D. Castro, T. Torfs, Q. Lin, C. van Hoof, G. Wang, Y. Lian, and N. van Helleputte, "A 400 GΩ input-impedance active electrode for non-contact capacitively coupled ECG acquisition with large linear-input-range and high CM-interference-tolerance," *IEEE Trans. Biomed. Circuits Syst.*, vol. 13, no. 2, pp. 376–386, Apr. 2019, doi: 10.1109/TBCAS.2019.2895660.

[15] *AD8505/AD8506/AD8508 Data Sheet, Revision 0*, Analog Devices, Norwood, MA, USA, Accessed: Jun. 13, 2022. [Online]. Available: https://www.analog.com/media/en/technical-documentation/data-sheets/AD8505_8506_8508.pdf

[16] M. Ker, "ESD (electrostatic discharge) protection design for nanoelectronics in CMOS technology," in *Proc. Adv. Signal. Process., Circuits Syst. Des. Tech. Commun.*, Kos, Greece, May 2006, pp. 217–279.

[17] *Electromagnetic Compatibility (EMC)—Part 4-2: Testing and Measurement Techniques—Electrostatic Discharge Immunity Test*, document IEC 61000-4-2:2008, TC 77/SC 77B, 2008.

[18] B. Russell. *Offset the Reduced ESD Protection of Netgen Nanometer ICs With off-Chip Alternatives*. Accessed: Sep. 13, 2007. [Online]. Available: https://www.embedded.com/offset-the-reduced-esd-protection-of-netgen-nanometer-ics-with-off-chip-alternatives/

[19] S. Marum, C. Duvvury, J. Park, A. Chadwick, and A. Jahanzeb, "Protecting circuits from the transient voltage suppressor's residual pulse during IEC 61000–4–2 stress," in *Proc. 31st EOS/ESD Symp.*, 2009, pp. 1–10.

[20] Qorvo Field Applications Team. *ESD Design Strategy for Mobile Devices: Your Tools Seed (Part 2 of 3)*. Accessed: Aug. 2, 2018. [Online]. Available: https://www.qorvo.com/design-hub/blog/esd-design-strategy-for-mobile-devices-your-tools-for-seed

[21] LLC. (Nov. 2018). *ESD7351, SZESD7351 Series, Revision. ON Semiconductor Component Industries*. Accessed: Jun. 13, 2022. [Online]. Available: https://www.onsemi.com/pdf/datasheet/esd7351-d.pdf

[22] P. K. Papastamatis, E. A. Paliatsos, I. F. Gonos, and I. A. Stathopulos, "Analysis of the ESD reconstruction methodology based on current probe measurements and frequency response compensation for different ESD generators and severity test levels," *Electronics*, vol. 10, no. 6, p. 728, Mar. 2021, doi: 10.3390/electronics10060728.

[23] G. P. Fotis, I. S. Stathopolus, and I. F. Gonos, "A current measurement procedure for the ESD generators according to the EN 61000–4–2," School Elect. Comput. Eng., Nat. Tech. Univ. Athens, Athens, Greece, Jan. 2004. [Online]. Available: http://users.ntua.gr/igonos/2004/CSCC2004-487-725.pdf

[24] C. Buaban, C. Ratametha, T. Limpisawas, T. Songthawornpong, B. Pholpoke, and W. Wattanapanitch, "A low-power high-input-impedance ECG readout system employing a very high-gain amplification and a signal-folding technique for dry-electrode recording," *IEEE Sensors J.*, vol. 21, no. 17, pp. 18905–18919, Sep. 2021, doi: 10.1109/JSEN.2021.3087723.

ROBERT CAMÓS-VIDAL was born in Girona, Spain, in December 1984. He received the first degree in industrial electronic technical engineering from Universitat de Girona, Girona, Spain, in 2009, and the second degree in electronic engineering degree from the Polytechnic University of Catalunya (UPC), Barcelona, Spain, in 2013, where he is currently pursuing the Ph.D. degree in electronic engineering with the Biomedical Research Center (CREB-UPC).

From 2010 to 2013, he was a Research Assistant with the Department of Industrial Engineering, CITCEA Technology Transfer Center, UPC. Over the last nine years, he was with two private companies as an research and development engineering team leader in the field of medical solutions in Girona. His research interest includes different application areas of medical devices, especially in health monitoring systems and non-invasive solutions.

JAVIER ROSELL-FERRER (Senior Member, IEEE) was born in Barcelona, Spain, in June 1959. He received the Ingeniero de Telecomunicación and Doctor Ingeniero de Telecomunicación degrees from the Polytechnic University of Catalunya (UPC), Barcelona, in 1983 and 1989, respectively.

He is currently a Full Professor with the Department of Electronic Engineering, UPC, where he is also the Head of a research group of the Biomedical Research Center (CREB-UPC). His current research interests include non-invasive and non-obtrusive measurement methods in sports, medical, and biological fields, particularly based on bio-electrical impedance spectroscopy and magnetic induction spectroscopy.